Planar Micro- and Nano-Patterning of GaN LEDs: Guidelines and Limitations

Johannes Herrnsdorf,[1, a)] Enyuan Xie,[1] Ian M. Watson,[1] Nicolas Laurand,[1] and Martin D. Dawson[1]
Institute of Photonics, University of Strathclyde, Glasgow G4 0NW, UK

(Dated: 17 January 2014)

The emission area of GaN light-emitting diodes can be patterned by etch-free current aperturing methods which exploit the thin and highly resistive nature of the p-doped layer in these devices. Here, the fundamental underlying electrical and optical aspects of high-resolution current aperturing are investigated theoretically. The most critical parameter for the possible resolution is the thickness d of the p-GaN layer, but the interplay of p-GaN resistivity and electrical junction characteristics is also important. A spatial resolution of $1.59d$ can in principle be achieved, corresponding to about 300 nm in typical epitaxial structures. Furthermore, the emission from such a small emitter will spread by about 600 nm while propagating through the p-GaN. Both values can be reduced by reducing d.

I. INTRODUCTION

Light-emitting diodes (LEDs) based on III-nitride materials are the subject of intensive research activity, mainly driven by their prospects as future lighting sources. Besides lighting, LEDs offer a wide range of potential applications including photo-excitation and optical manipulation tools for bio-photonics[1–3], high-bandwidth emitters for visible light communications[4–6], highly efficient colour conversion based on radiative or non-radiative transfer[7,8], maskless lithography methods[9] and micro-displays[8]. For many of these applications it is beneficial or even mandatory for the emitter to be patterned on a micron- or in some cases even on a sub-micron scale. Micro- and nano-sized emitters also offer opportunities to explore undiscovered device physics because they can be operated at much larger current densities than macroscopic devices[10]. The implications of high current density operation are the topic of ongoing research and relate to important challenges of III-nitride research, in particular carrier dynamics[11] and the so-called "efficiency droop"[12,13].

Most patterning techniques rely on etching methods. These become increasingly difficult as the pattern size is reduced to a few microns or less and, also, etching damage to the epitaxial structure often deteriorates device performance. Here, we will examine a different class of patterning techniques, the so-called "planar approach". This covers a whole range of techniques, all of which have in common that the LED mesa is macroscopic in size and the pattern is created by localizing the current injection into the p-GaN layer of the LED[6,9,14]. Such techniques tend to allow simpler fabrication of very small features compared to approaches based on etching and in GaAs-based infrared LEDs, sub-micron pattern definition was demonstrated in this way[15,16]. Localized current aperturing in III-nitride LEDs can be achieved for example by patterning the p-metal contact or by local variation of the contact resistivity between the current spreading layer and the p-GaN. In either case, patterns with at least sub-10-micron resolution are possible because the p-GaN layer is very thin and highly resistive, thus allowing only a small lateral spread of the injected hole-current before recombination in the junction region.

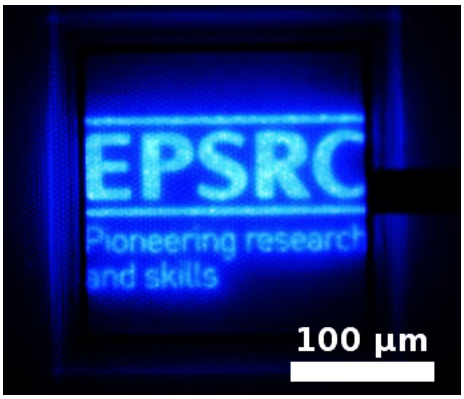

FIG. 1. Blue-emitting GaN LED with a pattern defined by current aperturing using the approach described in reference[9].

An example of an LED with a pattern created by current aperturing is shown in figure 1. In this particular case, the pattern was fabricated by localised plasma treatment as described by Massoubre *et al.*[9]. This involves application of a CHF_3-based plasma at room temperature, and has the advantages *(i)* that the effect of plasma treatment is blocked by conventional photoresist layers, allowing arbitrary micron-scale patterns to be defined, and *(ii)* that the plasma treatment penetrates through a conventional semi-transparent current spreading metal layer. Features of size $\sim 2\ \mu$m have successfully been defined in this way with potential for further improvement. This has motivated the present study.

Here, numerical methods are used to examine the fundamental electrical and optical properties of planar-patterned GaN LEDs with particular focus on the achievable spatial resolution. The current density within devices with current apertures is calculated in section II by a finite difference model and the emission is examined in section III by a finite difference time domain (FDTD) method. Both sections confirm that submicron features are in principle achievable but require the p-GaN layer

[a)] Electronic mail: johannes.herrnsdorf@strath.ac.uk

to be as thin as possible. It is expected that the smallest possible feature size is about 1.59× the p-GaN thickness. Whether this limit can be achieved depends not only on the fabrication limits of the current aperture, but also on the interplay between p-GaN resistivity and electrical characteristics of the junction at the operating voltage as well as in-well carrier diffusion.

II. CURRENT DENSITY DISTRIBUTION

A key aspect of pattern definition by current aperturing is the distribution of the current density within the device. Sophisticated models for this have been developed recently and were shown to accurately describe real existing devices[17–19]. Here, the current density is calculated by a finite difference model following a similar ansatz to that described by Bogdanov *et al.*[18]. Sections II A and II B explain the model. In sections II C and II D this model is used to explore the fundamental reasons for limitation of pattern resolution. Finally in section II E an analytical ansatz is developed based on the observations in the previous sections to derive the estimated resolution limit of 1.59× the p-GaN thickness.

A. Continuity Equation for Currents in the p- and n-GaN Layers

For our analysis, we divide the LED into three major sections, which are the n-doped layer, the p-doped layer and the junction region connecting the two. See figure 3a) below for an illustration. In the doped regions, the current densities $\vec{j}_{n,p}$ (where the subscript denotes the n- and p-doped regions) fulfil the continuity equations:

$$\vec{\nabla} \cdot \vec{j}_{n,p} = 0 \tag{1}$$

The current density vector here is given as the gradient of the Fermi level $F_{n,p}$

$$\vec{j}_{n,p} = \mu_{n,p} n_{n,p} \vec{\nabla} F_{n,p} \tag{2}$$

Where $\mu_{n,p}$ are the mobilities and $n_{n,p}$ are the carrier densities of the majority carrier in each region (contributions from minority carriers are ignored). Assuming that the spatial variation of these is negligible the Fermi-level therefore fulfils a homogeneous Poisson equation:

$$\nabla^2 F_{n,p} = 0 \tag{3}$$

At all semiconductor-air interfaces and at the interface of the n-GaN layer to the GaN buffer layer no current can leave the device, yielding homogeneous Neumann boundary conditions:

$$\vec{n} \cdot \vec{\nabla} F_{n,p}\Big|_{device\ boundary} = 0 \tag{4}$$

Equation (4) simply means that no carriers are crossing these boundaries. At the n- and p-metal contacts, Dirichlet boundary conditions are applied:

$$F_{n,p}|_{metal\ contact} = F_{n,p,contact} \tag{5}$$

Where we conveniently set $F_{n,contact} = 0$ and $F_{p,contact} = eV$, e is the elementary charge and V the voltage applied to the diode. It should be noted that this voltage V is actually a bit lower than the voltage applied to a real device because the contact resistivities are ignored. Spatial variation of V due to the resistivity of the spreading layer is assumed to be negligible for very small patterns as considered here. Planar approaches can typically be understood by simply assuming a patterned p-contact area. This is even true for techniques (such as localized plasma-treatment) that change the electrical properties of the p-GaN because the present understanding is that the p-GaN is only affected in a very thin layer (an order of magnitude thinner than the p-GaN thickness) directly at the top-surface[9].

A final boundary to equation (3) is given at the interface to the junction region. Following the suggestion by Bogdanov *et al.*[18], the junction is modeled seperately by a one-dimensional ansatz, i.e. only considering current components going perpendicularly through the junction. This yields an inhomogeneous Neumann boundary:

$$\vec{n} \cdot \vec{\nabla} F_{n,p}\Big|_{junction} = \frac{1}{\mu_{n,p} n_{n,p}} j_{z,jnct}(V_{jnct}) \tag{6}$$

$$V_{jnct} = F_{p,jnct} - F_{n,jnct} \tag{7}$$

Here, V_{jnct} corresponds to the voltage locally applied to the actual junction and $j_{z,jnct}$ is the response function of the junction to this voltage.

Equation (3) can be solved numerically using a finite difference method and a self-consistent iteration to account for the junction current. This is done in the three-dimensional numerical computations below (the self-consistent iteration was realized by an adapted binary search) which were done using Matlab™. See section I of the supplementary material[20] for full details of the numerical procedure. Analytical solutions are expected to be difficult and probably only possible in very few cases, e.g. below in section II E.

B. Material Parameters

As will be shown, a factor of crucial importance is the conductivity of the p-GaN. Two extreme cases will be examined: A highly conductive p-GaN representing the state of the art on one hand and on the other hand highly resistive p-GaN. The first case is given by[21]:

$$\mu_p = 30\ \mathrm{cm}^2/\mathrm{Vs} \qquad n_p = 5 \times 10^{17}\ \mathrm{cm}^{-3} \tag{8}$$

The poorly conductive p-GaN is given by:

$$\mu_p = 1\ \mathrm{cm}^2/\mathrm{Vs} \qquad n_p = 10^{17}\ \mathrm{cm}^{-3} \tag{9}$$

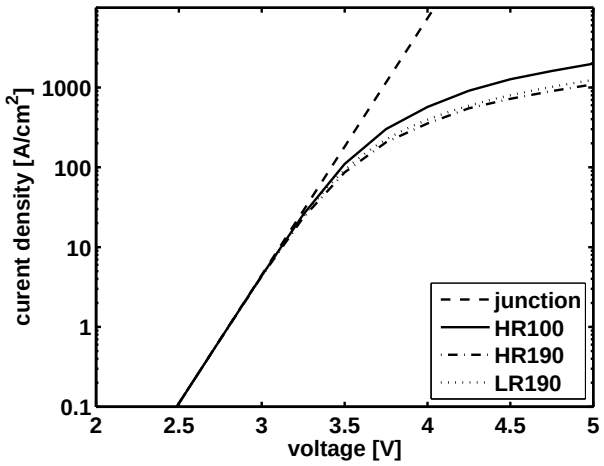

FIG. 2. *I-V* characteristics of the junction according to equation (11) and of unpatterned LEDs with a 10×10 μm^2 mesa. Note that the curves of the HR190 and LR190 devices are hardly distinguishable on the scale of this graph.

For the n-GaN, the following values are taken throughout:

$$\mu_n = 2000 \text{ cm}^2/\text{Vs} \qquad n_n = 5 \times 10^{18} \text{ cm}^{-3} \tag{10}$$

In the above, $\mu_{n,p}$ represents the mobility and $n_{n,p}$ the carrier density (activated dopant density). These values may exaggerate the conductivity contrast between p- and n-GaN in comparison to real devices. For reference, some key results were reproduced with an electron mobility of $\mu_n = 200$ cm^2/Vs and are commented on in section II of the supplementary material[20].

In a first approximation, the junction current in equation (6) may be described by an exponential law:

$$j_{z,jnct}(V_{jnct}) = j_{sat}\left(\exp\left(\frac{V_{jnct}}{nkT}\right) - 1\right) \tag{11}$$

where j_{sat} is the diode saturation current, T the junction temperature, k the Boltzmann constant and n the ideality factor. A resistance ρ in series with the ideal diode can be described by a set of coupled equations:

$$j_{z,jnct} = j_{sat}\left(\exp\left(\frac{V_{jnct} - V'}{nkT}\right) - 1\right) \tag{12a}$$

$$V' = \rho j_{sat}\left(\exp\left(\frac{V_{jnct} - V'}{nkT}\right) - 1\right) \tag{12b}$$

Unless specified otherwise, the following parameters are used for equations (11) and (12):

$$\begin{aligned} j_{sat} &= 10^{-9} \text{ A/cm}^2 \qquad n = 5 \\ \rho &= 10^{-3} \ \Omega\text{cm}^2 \qquad kT = 27 \text{ meV} \end{aligned} \tag{13}$$

GaN based diodes behave as ideal diodes (with high ideality factors) only for voltages that do not much exceed the turn-on voltage. Above this, significant parasitic resistances in series with the ideal diode characteristics have to be considered. These originate from the contact resistances (not considered in the model), the resistivity of p- and n-GaN and the junction region itself[21]. In this article we compare the two opposing cases of poorly conductive p-GaN and ideal junction characteristics on one hand and highly conductive p-GaN and a resistive junction on the other hand. In particular, the following device types are considered:

- **HR190**: having a 190 nm thick p-GaN layer with high resistivity given by equation (9) and an exponential junction behavior given by equations (11) and (13).
- **HR100**: same as HR190 but with a p-GaN thickness of 100 nm
- **HR190II**: same as HR190 but with an ideality factor of $n = 4.5$
- **LR190**: having a 190 nm thick p-GaN layer with low resistivity given by equation (8) and a resistive junction behavior given by equations (12) and (13).

Calculated current-voltage (*I-V*) characteristics of LED micro-mesas with these parameters are shown in figure 2. In the displayed voltage regime they mimic experimentally observed characteristics of real micro-LEDs (see e.g. Gong *et al.*[10] for experimental curves). It should be emphasized at this point that it is not the intention of this work to accurately model existing devices but to gain insight into fundamental principles. Note that the parameters are chosen such that an unpatterned micro-LED of type HR190 has almost the same *I-V* behavior as a micro-LED of type LR190, thus allowing a fair comparison. It will be demonstrated and discussed below that the HR-type devices allow a better spatial resolution.

C. Fundamental Observation: Lateral Currents in the p-GaN Layer

To obtain a first understanding of the current distribution in a device, we consider a device of type LR190 in the format of a 5×5 μm^2 LED mesa with a 1 μm wide stripe-shaped p-contact and n-contacts to either side. A schematic of this layout is shown in figure 3. The mesa height was 2 μm, the p-GaN thickness 190 nm and the overall n-GaN thickness 3 μm (see figure 3a) for a schematic showing these layers). For comparison, a mesa height of only 1 μm was considered as well but no difference in the results was seen. A voltage of 4.5 V was applied between the p- and n-contact areas.

The calculated current density distribution is shown in figure 4. Current crowding effects can be seen at the edges of both n- and p-metal contacts. In particular, in the p-GaN layer the x-component of the current density vector shown in figure 4a) contains strong lateral currents of several kA/cm^2 leading away from the edges of the

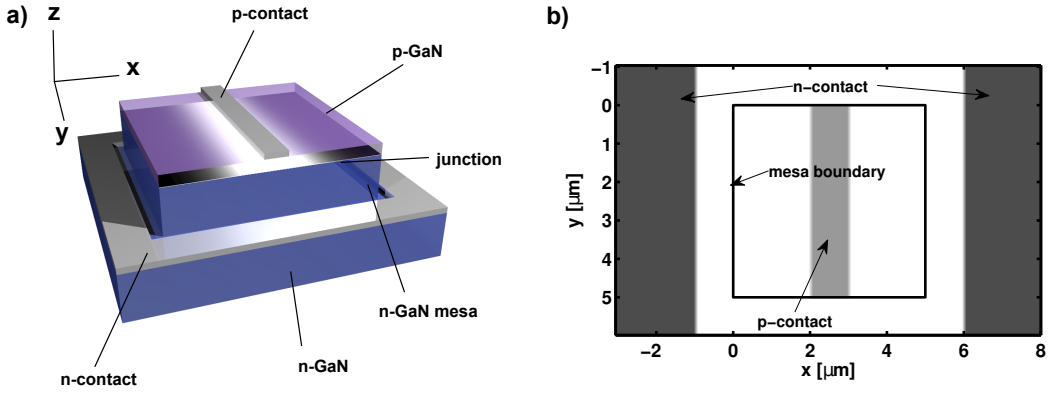

FIG. 3. Schematic of the LED structure considered: *a)* 3D-view, not to scale, *b)* top-view to scale of the structure used in section II C.

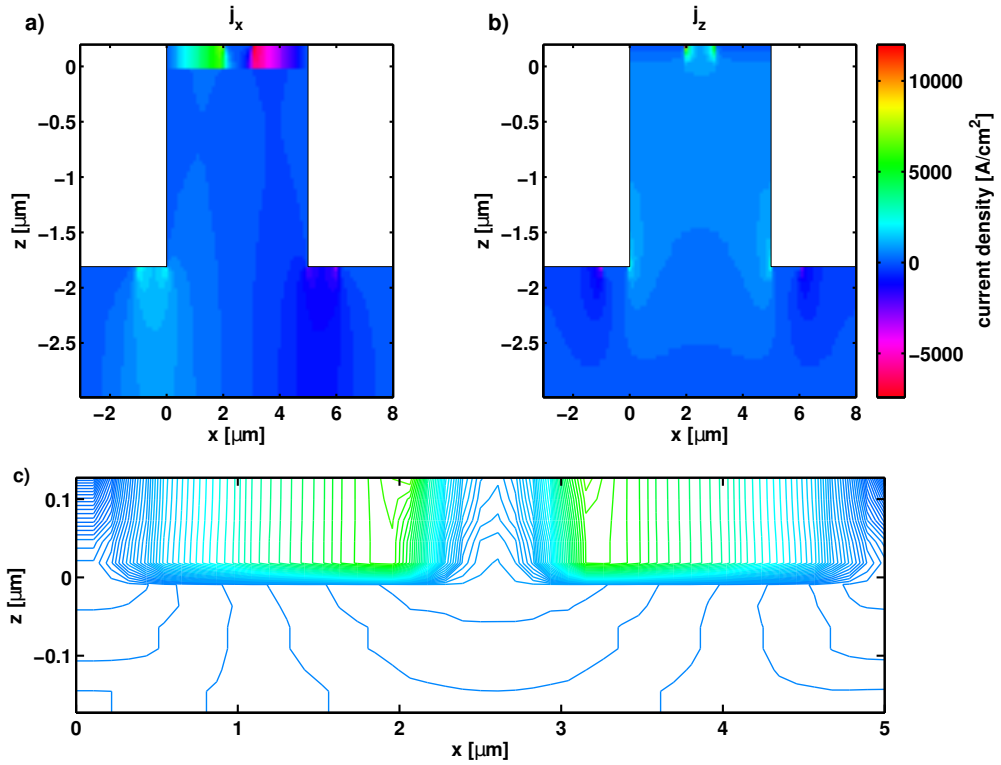

FIG. 4. Cross section at $y = 2.5$ μm through the device shown in figure 3b) showing different components of the current density vector. The maps show the calculated *a)* x-component (currents going from left to right) and *b)* z-component (currents going from bottom to top). The y-component (currents going vertical to the cross-section plane) is not displayed because it is at least two orders of magnitude smaller than the x- and z-components. A detailed view of the overall current density (length of the current density vector) in the region close to the junction is given in the contour map *c)*. The color bar next to sub-figure *b)* applies to all sub-figures.

stripe. These exceed the maximum junction current (ca. 700 A/cm^2, see figure 5) by an order of magnitude. The detailed view of the region close to the junction shown in figure 4c) demonstrates that this effect is indeed confined to the p-GaN layer. A consequence of these lateral currents is a significant spatial spread of the current going through the junction, i.e. a loss in resolution. Indeed, the junction current mapped in figure 5 does not drop to half its maximum value within the mesa. Accordingly, the voltage applied to the junction changes only by a very small amount between mesa center and boundary. This is a result of the current being limited mainly by the junction itself and not by the resistivity of the p-GaN, i.e. compared to the p- and n-GaN layers the junction behaves almost like an insulator.

According to equation (2), the current density in the

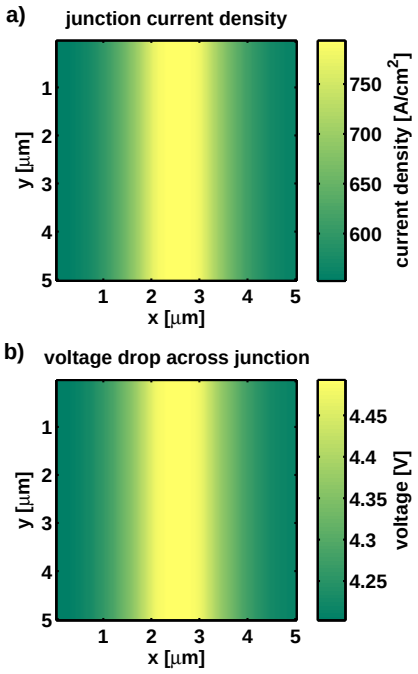

FIG. 5. Maps of the *a)* current density going through the junction and *b)* voltage applied to the junction of the microstripe device shown in figure 3b).

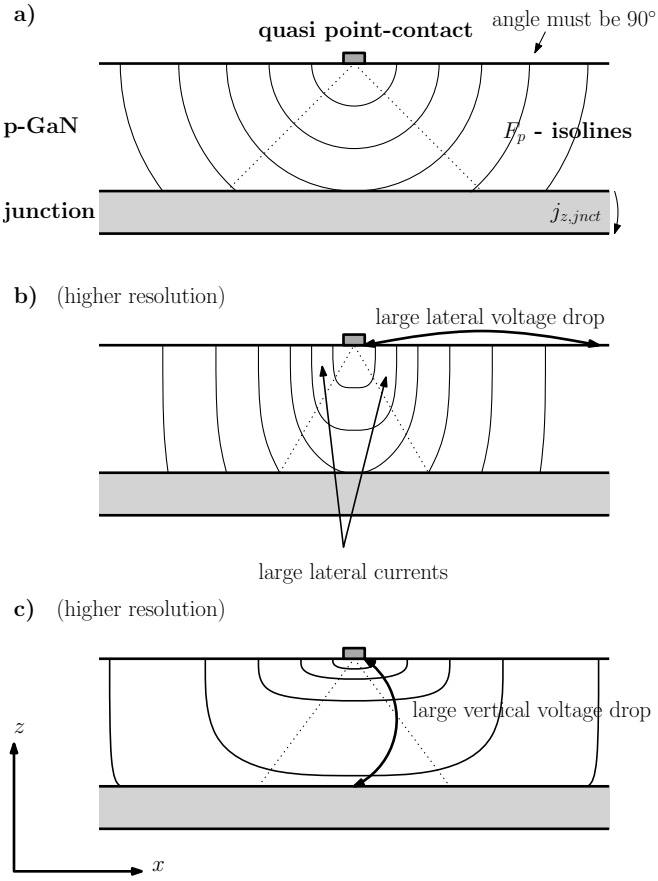

FIG. 6. Illustration of the possible distribution of F_p in the p-GaN layer. Case *a)* represents the case where (14) is fulfilled with equal voltage drop in any direction. Cases *b)* and *c)* are possible scenarios where the full width half maximum of $j_{z,jnct}$ is smaller than in *a)*. Scenario *b)* is characterized by a large lateral voltage drop and scenario *c)* by a large vertical voltage drop. The dotted lines illustrate the lateral spread of the j_z current.

p-GaN is given by the gradient of F_p. Therefore, a very basic schematic of the distribution of F_p in the p-GaN layer is drawn in figure 6 in the case of a very small (compared to the p-GaN thickness) p-contact. Here, F_p is indicated by isolines and due to the boundary condition (4) these have to meet the p-GaN/air interface at an angle of 90°, as indicated in figure 6a). In the theoretical limit of an infinitely large LED mesa, the voltage drop across the junction will approach 0 for $x \to \pm\infty$ in figure 6. This means that $F_{p,jnct}$ will drop towards $F_{n,jnct}$ (note that the point where $F_{p,jnct} \approx F_{n,jnct}$ may be well beyond the size of any real mesa). Since p-GaN has a much higher resistivity, most of this drop will be in the p-GaN and only an insignificant variance of $F_{n,jnct}$ in the n-GaN is expected. These two conditions, i.e. that $F_{p,jnct}$ must change along x and that the F_p isolines have to be at 90° angle to the p-GaN/air interface, mean that there are inevitably lateral currents in the p-GaN layer.

Such unavoidable lateral currents will of course have an impact on the achievable pattern resolution. In the following sections it will be discussed how electrical properties of the device and LED geometry influence this relationship. A coarse, graphical insight can already be gained at this stage. Figures 6b) and c) illustrate how the F_p distribution might be in a device which has the same device geometry as figure 6a) but higher pattern resolution. Since $j_{z,jnct}$ is driven by $F_{p,jnct} - F_{n,jnct}$, a high resolution requires $F_{p,jnct}$ to drop quickly with x. The F_p-isolines in figure 6b) and c) are drawn accordingly. Two possibilities are shown: a quick lateral drop of F_p towards F_n in case b) and a large vertical voltage drop in case c). Simulations below suggest that case c) is achievable in real devices. It has similar or even lower lateral currents than case a) but much higher current in z-direction close to the point of injection.

D. Achieving Sub-Micron Resolution

Experimentally, significantly better resolution and contrast than shown in figure 5 for the LR190 microstripe device has been reported[9,16]. To understand how this is possible we consider a device with nano-point current injection. In this case, the LED mesa was 4×4 μm^2, the mesa height 2 μm and the overall n-GaN thickness 3 μm. A circular p-contact of 100 nm diameter was defined in the center of the mesa and the mesa was surrounded on all sides by the n-contact. A schematic of the device is

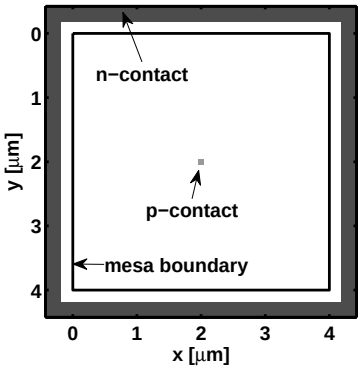

FIG. 7. Schematic of the device layout with nano-point current injection. Compare also figure 3.

shown in figure 7.

Devices with this layout but different p-GaN and junction characteristics were modeled for externally applied voltages ranging from 0.5 V to 5 V. Voltage dependent peak current density and full width half maximum (FWHM) of the junction current in lateral direction are plotted in figure 8. We make the following observations:

- In comparison to figure 2, the highest current density in the nanopoint structure at a given voltage (above turn-on) is about 5× lower than for the unpatterned micro-LED.
  - This is attributed to the lateral spread of the current in the nanopoint device, which is not possible for a mesa that is entirely covered by the p-contact.
- In the devices with highly resistive p-GaN (HR$\cdots$), the voltage at which the p-GaN conductivity starts to determine the *I-V* characteristics is lower in the nanopoint device (ca. 2.5 V as opposed to 3 V for the unpatterned HR190 device).
  - Below this voltage, the current injected at the quasi-point contact spreads across the whole junction region, above it confines to a small spatial region. At high operation voltages (5 V) the FWHM converges to approximately 250 nm (HR190 and HR190II) and 120 nm (HR100), respectively.
  - The FWHM as a function of peak current is the same for devices HR190 and HR190II (an explanation is given below in section II E).
- Device LR190 has a FWHM of 2 μm at 5 V. For most voltages considered, the current is spread out across the entire mesa.

An immediate conclusion is that the possible resolution is determined by the interplay of p-GaN conductivity and the junction characteristics as well as the p-GaN thickness.

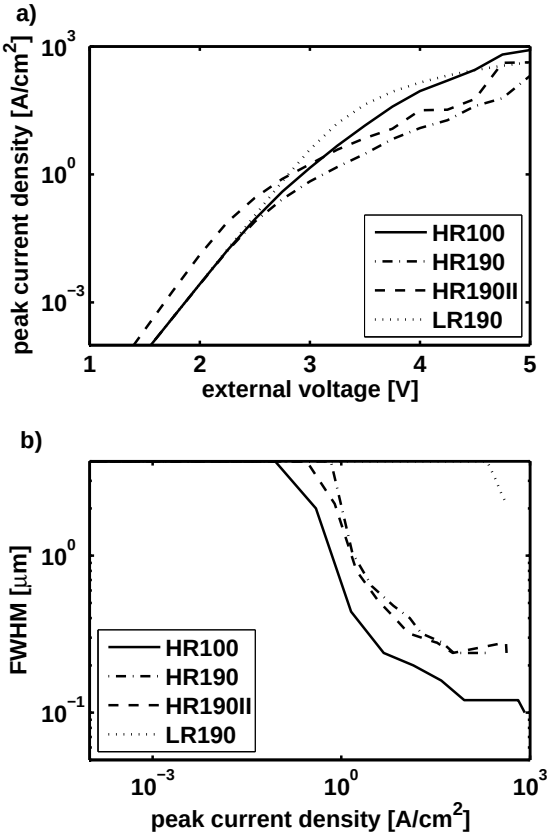

FIG. 8. *a) I-V* characteristic and *b)* FWHM of the spatial spread of $j_{z,jnct}$ for a nanopoint structure (figure 7) with different different device types as described in section II B. Compare figure 2 for corresponding *I-V* curves of a conventional micro-mesa LED.

Let us look at the lateral distribution of the junction current and the voltage applied to the junction region. These are plotted in figure 9 for the HR190 device. It can be seen that at low external voltage, the junction voltage is practically the same as the external voltage and both junction voltage and current are almost uniform across the whole mesa, i.e. the junction behaves like an insulator. At higher external voltage, the voltage applied to the junction drops significantly with respect to the external voltage. This is caused by the voltage drop across the highly resistive p-GaN as more and more current is flowing through the device. Still, the spatial variation of the junction voltage is fairly shallow, on the order of 10 %. This shows that in this device, the voltage and current distribution in the p-GaN layer follow a pattern as indicated above in figure 6c). Generally, for all devices modeled in this work the junction voltage varied only by a small amount, i.e. the case shown in figure 6b) was never observed. Despite only modest variation of the junction voltage, the junction current in device HR190 is

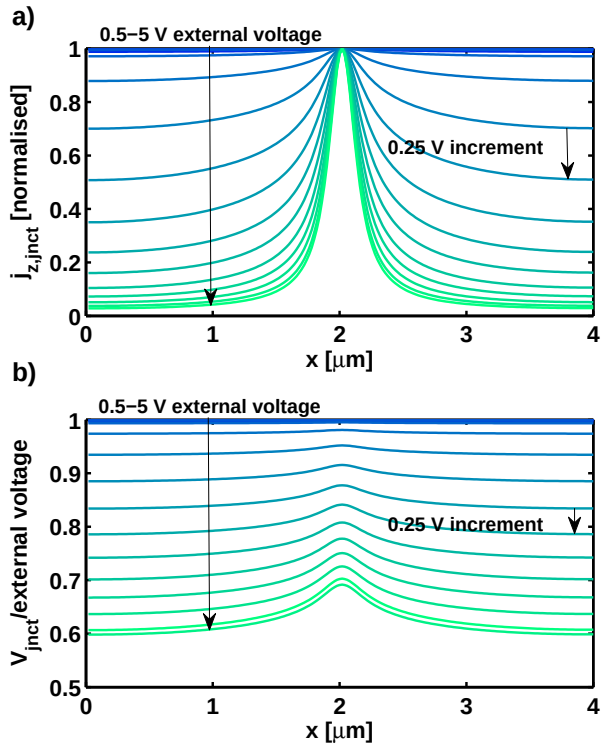

FIG. 9. Cross section plots of *a)* junction current and *b)* junction voltage through the center of an HR190 nano-point structure (figure 7). The difference of externally applied voltage between adjacent curves is 0.25 V.

strongly confined at high voltages which is a result of the strong non-linearity of the junction I-V behavior.

The conclusions of this section are that, in devices patterned by current aperturing, the junction voltage varies only by a small amount and high resolution is achieved if the response of the junction to this shallow voltage variation is strongly non-linear. Furthermore, current confinement is only observed if the resistance of the p-GaN layer at the operating voltage is of comparable order or higher than that of the junction, i.e. there is a significant voltage drop across the p-GaN layer. This means that pattern resolution can in principle be improved by decreasing the p-GaN conductivity, diode ideality factor and parasitic resistances within the junction. The limits of resolution improvement by this approach are discussed below in section II E.

E. Analytical Estimate of the Possible Resolution

The p-GaN conductivity is much lower than that of n-GaN. We can exploit this by noting that the voltage drop basically occurs in across the p-GaN and the junction, i.e. we can in good approximation say that $F_n \approx 0$ in the whole n-GaN region. In the highly idealized case of an infinitely small point contact, an infinitely thick p-GaN and an infinitely large mesa the analytical solution of equation (3) in the p-GaN layer is known:

$$F_p = \frac{q}{\sqrt{x_\perp^2 + z^2}} \tag{14}$$

Where $x_\perp$ is a lateral displacement relative to the position of the point source in any direction within the $x-y$ plane and q is a proportionality constant and mathematically equivalent to a charge in electrostatic theory.

Above, it was demonstrated that high resolution devices have a very shallow modulation of the junction voltage and the pattern is generated by the highly non-linear response of the junction. To obtain an analytical estimate of the resolution limit, we look at the limit of an infinitely strong junction response, i.e. the pattern is generated by an infinitely small variation of the junction voltage. This means, that $F_{p,jnct}$ is constant (without loss of generality $F_{p,jnct} = 0$). On this basis, we can replace equation (14) by a more accurate expression for F_p:

$$\begin{aligned} F_p = \frac{q}{d}\Bigg(&\frac{1}{\sqrt{X^2+Z^2}} \\ &+\sum_{i=1}^{\infty}(-1)^i\left[\frac{1}{\sqrt{X^2+(Z+2(i+1))^2}}\right. \\ &\left.+\frac{1}{\sqrt{X^2+(Z-2(i+1))^2}}\right]\Bigg) \end{aligned} \tag{15}$$

$$X = \frac{x_\perp}{d} \tag{16}$$

$$Z = \frac{z}{d} \tag{17}$$

See section III of the supplementary material[20] for a derivation of equation (15) using the image charge technique. The junction current is then given by:

$$\begin{aligned} j_{z,jnct} &= \mu_p n_p \left.\frac{\partial F_p}{\partial z}\right|_{z=d} \\ &= -\frac{\mu_p n_p q}{d^2}\Bigg(\frac{1}{(X^2+1)^{3/2}} \\ &\quad+\sum_{i=1}^{\infty}(-1)^i\left[\frac{2i+3}{(X^2+(2i+3)^2)^{3/2}}\right. \\ &\quad\left.-\frac{2i+1}{(X^2+(2i+1)^2)^{3/2}}\right]\Bigg) \end{aligned} \tag{18}$$

The FWHM of the spatial spread of the junction current is given by the condition:

$$\begin{aligned} 0 &= 2j_{z,jnct}(\delta) - j_{z,jnct}(0) \\ &= \frac{2}{(\delta^2+1)^{3/2}} - 1 \\ &\quad+\sum_{i=1}^{\infty}(-1)^i\left[\frac{4i+6}{(\delta^2+(2i+3))^{3/2}} - \frac{4i+2}{(\delta^2+(2i+1))^{3/2}}\right. \\ &\quad\left.-\frac{1}{(2i+3)^2}+\frac{1}{(2i+1)^2}\right] \end{aligned} \tag{19}$$

Equation (19) was solved numerically using the `fzero` function of Matlab^{TM}. A value of $\delta = 0.79$ was found, yielding a resolution limit of:

$$\text{FWHM} = 2\delta d = 1.59d \tag{20}$$

Equation (20) represents the limit that can be achieved by lowering the p-GaN conductivity and increasing junction response in the ideal case of a point source. Once a device operates at the resolution given by (20), further decrease of p-GaN conductivity or ideality factor will not result in a better resolution. This is why in figure 8 devices HR190 ($n = 5$) and HR190II ($n = 4.5$) have identical resolution.

F. In-Well Diffusion of Carriers

Once the carriers have been injected into the junction region, they reside in the quantum wells for a lifetime on the order of 10 ns. In this time, carrier diffusion will cause a further spatial spread of the two-dimensional electron and hole gas within the quantum wells. Previous work by Sonderegger *et al.*[22] suggests that this spread is on the order of 100 nm which is significant in particular for thin p-GaN structures.

III. SPREAD OF OPTICAL EMISSION

Above in section II the size of the emitter given by the spread of the of the injected current was discussed. This by itself is important e.g. for fundamental small-emitter physics or individual addressing of small structures (e.g. epitaxial quantum dots) within the junction region. However, the emitter is still situated at a significant distance from the device surface, allowing emitted light to spread to a size that is potentially significantly larger than the original emitter size. This effect is important for some potential applications such as contact lithography or localized excitation of colour-converting overlayers. Therefore, the spread of emission upon propagation to the device surface was investigated by FDTD calculations.

A. Device Structure

A very simple LED structure is assumed: the n-GaN and GaN buffer layers are assumed to be infinitely thick, the QW region infinitely thin and the p-GaN layer to have a thickness d. Unless specified otherwise, a value of $d = 190$ nm was used. On top is a 100 nm thick indium tin oxide (ITO) current spreading layer. On top of the ITO layer is air/vacuum. A schematic is shown in figure 10. Different types of current spreading materials may be used, e.g. thin metallic films or alloys[9]. Alloys are very difficult to consider in this type of model because of their complex nature which involes significant effects from random alignment of phases, partial oxidation and porosity. For comparison with the ITO simulation, a thin metallic current spreading layer made from 30 nm Pd was modelled as well. The results are generally very similar to those with the ITO layer. See section IV.B of the supplementary material[20] for the corresponding simulation data.

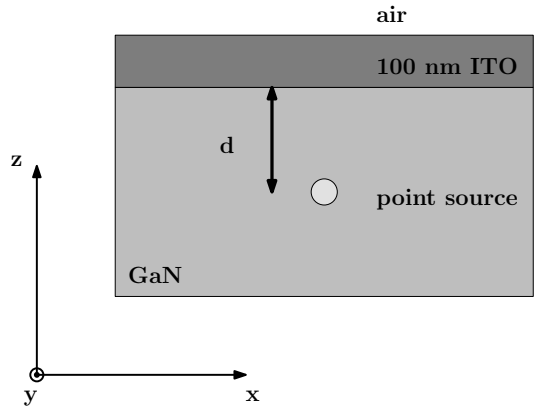

FIG. 10. Schematic of the device structure for FDTD modeling.

B. Numerical Method

FDTD calculations were done using the software package "meep"[23] in a rectangular computational cell (4×4 μm in the 2D case and $1.25\times1.25\times1$ μm in the 3D case). All GaN layers were taken to have a uniform dielectric constant of $\epsilon = 6.1848$. ITO was represented as a loss-less material with dielectric constant $\epsilon = 4$ and for Pd optical properties reported by Radić *et al.*[24] were used.

A linearly polarized CW point source emitting at 450 nm with a was placed in the QW region. Each of the three possible polarization directions of the source was considered individually. In the figures below, the optical field energy averaged over one optical period is shown. See section IV.A of the supplementary material[20] for further details of the numerical procedure.

C. Results

In a first instance, a 2D model was implemented. Calculated optical field intensities are shown in figure 11. It is observed that radiation with z-polarized electric field has only evanescent components outside the sample, whereas the other two polarization directions radiate into the far field. In any case, the FWHM of the optical field energy at the sample surface is on the order of a micron.

Then, the model was extended to a full 3D representation of the device. The findings in this case are first

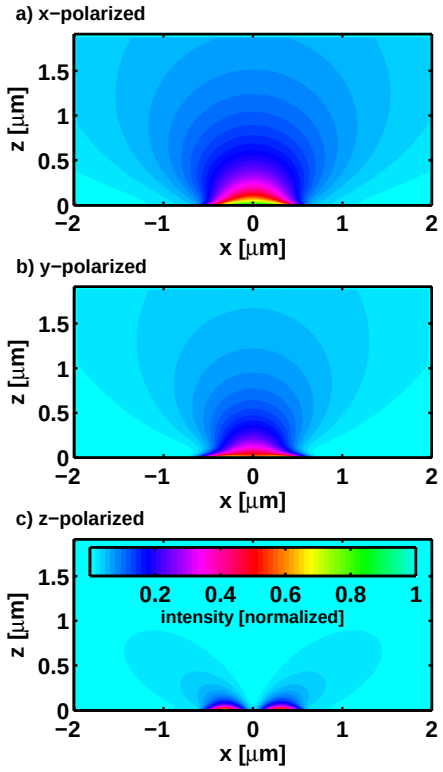

FIG. 11. Field intensity maps above the device surface in 2D simulation, where the light source was linearly polarized in *a)* x-, *b)* y- and *c)* z- direction. See figure 10 for definition the x, y- and z- directions. The color bar given in sub-figure *c)* applies to all sub-figures.

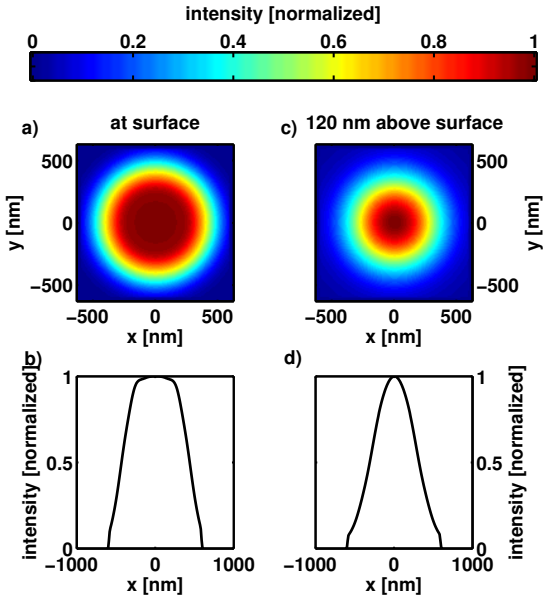

FIG. 12. Emission pattern (*a)* and *c)*) and cross section (*b)* and *d)*) in 3D simulation where contributions from x-, y- and z- polarized sources are summed. *a)* and *b)* are directly at the sample surface and *c)* and *d)* are 120 nm above it.

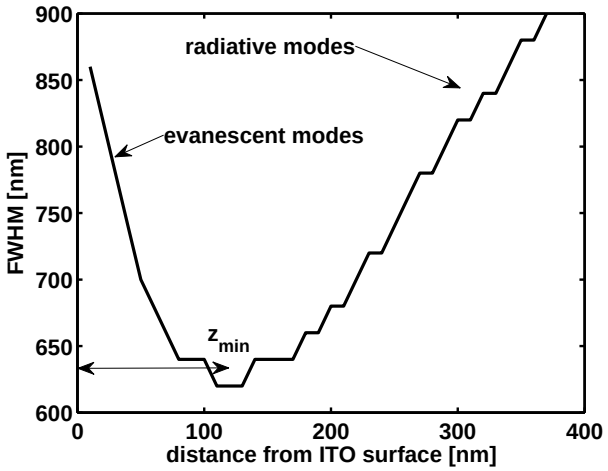

FIG. 13. Evolution of the lateral (i.e. in-plane with the sample surface) FWHM of the emission in 3D simulation. Here, the field energies of all three polarization components are summed. The p-GaN thickness is $d = 190$ nm (compare figure 14).

illustrated on the example of a p-GaN layer thickness of $d = 190$ nm. Then the influence of the p-GaN layer thickness is examined. As in the 2D case, emission with z-polarized electric field is evanescent outside the sample whereas the other two polarization components radiate into the far field. Figure 12 shows intensity maps and cross sections considering the contributions of all three polarization components which are taken to be equal. The field intensity is plotted directly at the sample surface and 120 nm above it. Surprisingly, the FWHM is reduced at a small distance from the surface. This is due to the decay of the evanescent modes which make up most of the broadening directly at the sample surface. When moving further away from the surface, the FWHM increases again due to the divergence of the radiative modes. Figure 13 shows the dependence of the FWHM on the distance from the sample surface. Up to a distance of about 400 nm, the FWHM is sub-micron with a minimum of 620 nm at a distance of $z_{min} = 120$ nm.

In general, for each value of the p-GaN layer thickness, d, there is a certain distance z_{min} from the sample surface at which the FWHM of the emission pattern is minimal. The values of z_{min} as a function of d and the corresponding FWHM are plotted in figure 14. The minimum p-GaN layer thickness considered here is 50 nm because thinner layers may not be practical due to the depletion width required in the p-GaN which was estimated e.g. by Kwon *et al.*[25] to be 76 nm. Typical epitaxial structures with a p-GaN thickness near 200 nm have a minimum FWHM of about 600 nm and z_{min} ≈120 nm. Similar values were found with Pd instead of ITO. By thinning the p-GaN to less than 100 nm it is possible to reduce

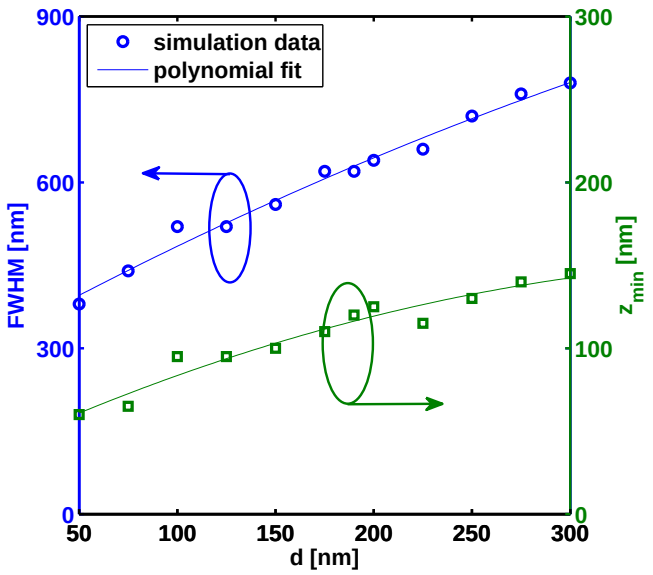

FIG. 14. Achievable FWHM of the emission as a function of p-GaN thickness and the distance z_{min} from the sample surface at which this FWHM is found (compare also figure 13). The solid lines are fits with a second order polynomial and serve as a guide to the eye.

the FWHM to 400 nm at a slightly shorter z_{min} ≈80 nm. In the case of Pd, the minimal FWHM is 250 nm directly at the sample surface.

In the case of a finite emitter size, the apparent size at the sample surface will be given by the convolution of the the emitter shape and the above results.

IV. CONCLUSION

Current aperturing at the p-contact area of GaN LEDs can in principle be used to define sub-micron sized emission patterns. Parameters determining the possible resolution are the p-GaN thickness and the interplay of p-GaN resistivity and junction characteristics at the operating voltage. The characteristics of the n-GaN do not significantly influence the resolution as long as there is a strong resistivity contrast to the p-GaN. Constraints to the achievable resolution arise from the lateral spread of the injected current while passing through the p-GaN and also from the divergence of the emission while propagating through the p-GaN layer.

The lateral current spread was investigated with a finite differences method. It was found that patterns with a best resolution of $1.59d$ (where d is the p-GaN thickness) can be achieved in devices where:

- The junction voltage is almost constant and only varies by a relatively small amount.
- The junction current depends strongly non-linearly on the junction voltage and thus the small modulation of junction voltage leads to a strong variation of the junction current.
- The p-GaN resistivity is sufficiently high to warrant a significant voltage drop across the p-GaN layer, i.e. the overall resistance of the p-GaN layer needs to be significant.

This resolution limit given by the current spread is relevant for any application that relies on addressing small areas within the active region, e.g. high current density operation or individual electrical addressing of nanostructures. For a typical epitaxial structure ($d = 190$ nm) this limit is 300 nm but it can in principle be reduced to 80 nm by using a p-GaN thickness of only 50 nm. Thinner p-GaN layers may require higher p-GaN resistivity in order to keep the overall resistance of the layer at a significant level. It should be noted that this spot size is subject to further in-well diffusion by approximately 100 nm.

Even if a nano-LED is created, i.e. an emissive region within the junction of sub-100 nm size, its emission outside the sample will have spread to a spot size of a few hundred nanometers. This is the practical resolution limit of this approach for applications that make use of the light field near the sample surface (e.g. contact lithography or color conversion). In the case of conventional epitaxial structures this optical resolution limit is about 600 nm. By using thin p-GaN layers with less than 100 nm thickness, a better resolution of about 400 nm is possible. Furthermore, by using a thin metallic current spreading layer, 250 nm optical resolution may be achievable. It should also be noted that this is the minimum spot size that is expected to be found by techniques like scanning near field microscopy, i.e. for nano-emitters fabricated by this approach *even scanning near field microscopy will not reveal the true size.*

ACKNOWLEDGMENTS

The authors thank EPSRC for funding under the UP-VLC grant (EP/K00042X/1), http://up-vlc.photonics.ac.uk/.

[1] N. Grossman, V. Poher, M. S. Grubb, G. T. Kennedy, K. Nikolic, B. McGovern, R. B. Palmini, Z. Gong, E. M. Drakakis, M. A. A. Neil, M. D. Dawson, J. Burrone, and P. Degenaar, J. Neural Eng. **7**, 016004 (2010)
[2] P. Y. Chiou, A. T. Ohta, and M. C. Wu, Nature **436**, 370 (2005)
[3] A. Zarowna-Dabrowska, S. L. Neale, D. Massoubre, J. McKendry, B. R. Rae, R. K. Henderson, M. J. Rose, H. Yin, J. M. Cooper, E. Gu, and M. D. Dawson, Opt. Express **19**, 2720 (2011)
[4] T. Komine and M. Nakagawa, IEEE Trans. Consumer Electron. **50**, 100 (2004)
[5] J. J. D. McKendry, D. Massoubre, S. Zhang, B. R. Rae, R. P. Green, E. Gu, R. K. Henderson, A. E. Kelly, and M. D. Dawson, J. Lightwave Technol. **30**, 61 (2012)
[6] C.-L. Liao, Y.-F. Chang, C.-L. Ho, and M.-C. Wu, IEEE Electron Dev. Lett. **34**, 611 (2013)
[7] S. Chanyawadee, P. G. Lagoudakis, R. T. Harley, M. D. B. Charlton, D. V. Talapin, H. W. Huang, and C.-H. Lin, Adv. Mater. **22**, 602 (2010)

[8]Z. Gong, E. Gu, S. Jin, D. Massoubre, B. Guilhabert, H. Zhang, M. Dawson, V. Poher, G. Kennedy, P. French, and M. Neil, J. Phys. D: Appl. Phys. **41**, 094002 (2008)
[9]D. Massoubre, E. Xie, B. Guilhabert, J. Herrnsdorf, E. Gu, I. M. Watson, and M. D. Dawson, Semicond. Sci. Technol. **29**, 015005 (2014)
[10]Z. Gong, S. Jin, Y. Chen, J. McKendry, D. Massoubre, I. M. Watson, E. Gu, and M. D. Dawson, J. Appl. Phys. **107**, 013103 (2010)
[11]R. P. Green, J. J. D. McKendry, D. Massoubre, E. Gu, and M. D. Dawson, Appl. Phys. Lett. **102**, 091103 (2013)
[12]J. Piprek, Phys. Status Solidi A **207**, 2217 (2010)
[13]P. Tian, J. J. D. McKendry, Z. Gong, B. Guilhabert, I. M. Watson, E. Gu, Z. Chen, G. Zhang, and M. D. Dawson, Appl. Phys. Lett. **101**, 231110 (2012)
[14]T.-W. Kuo, S.-X. Lin, P.-K. Hung, K.-K. Chong, C.-I. Hung, and M.-P. Houng, Jpn. J. Appl. Phys. **49**, 116504 (2010)
[15]O. Makarovsky, S. Kumar, A. Rastelli, A. Patanè, L. Eaves, A. G. Balanov, O. G. Schmidt, R. Campion, and C. T. Foxon, Adv. Mater. **22**, 3176 (2010)
[16]F. Intonti, V. Matarazzo, A. Nasir, O. Makarovsky, R. Campion, A. Patanè, S. Kumar, A. Rastelli, O. G. Schmidt, and M. Gurioli, Appl. Phys. Lett. **98**, 183102 (2011)
[17]X. Guo and E. F. Schubert, Appl. Phys. Lett. **78**, 3337 (2001)
[18]M. V. Bogdanov, K. A. Bulashevich, I. Y. Evstratov, A. I. Zhmakin, and S. Y. Karpov, Semicond. Sci. Technol. **23**, 125023 (2008)
[19]A. E. Chernyakov, K. A. Bulashevich, S. Y. Karpov, and A. L. Zakgeim, Phys. Status Solidi A **210**, 466 (2013)
[20]See supplementary material at [URL will be inserted by AIP] for additional results and further details on the methods used in the main article.
[21]E. F. Schubert, *Light-Emitting Diodes*, 2nd ed. (Cambridge University Press, 2006)
[22]S. Sonderegger, E. Feltin, M. Merano, A. Crottini, J. F. Carlin, R. Sachot, B. Deveaud, N. Grandjean, and J. D. Garnière, Appl. Phys. Lett. **89**, 232109 (2006)
[23]A. F. Oskooi, D. Roundy, M. Ibanescu, P. Bermel, J. D. Joannopoulos, and S. G. Johnson, Computer Physics Communications **181**, 687 (2010)
[24]A. D. Radić, A. B. Djurišić, J. M. Elazar, and M. L. Majewski, Appl. Opt. **37**, 5271 (1998)
[25]M.-K. Kwon, J.-Y. Kim, B.-H. Kim, I.-K. Park, C.-Y. Cho, C. C. Byeon, and S.-J. Park, Adv. Mater. **20**, 1253 (2008)